电 化 学
J. Electrochem. 2022, 28(8), 2201241 (1 of 10)

[Article] DOI: 10.13208/j.electrochem.220124 Http://electrochem.xmu.edu.cn

Low-Crystallinity and Heterostructured AuPt-Ru@CNTs as Highly Efficient Multifunctional Electrocatalyst

Tuan-Jie Gan[1], Jian-Ping Wu[1], Shi Liu[2], Wen-Jun Ou[2], Bin Ling[2], Xiong-Wu Kang[2*]

(*1. Jiangmen Power Supply Bureau of Guangdong Power Grid Co., Ltd, 152, Jianshe Second Road, Jiangmen 529030, Guangdong, China; 2. Guangdong Huihydrogen Energy Technology Co., Ltd, 808 Dongfeng East Road, Meihuacun Street, Guangzhou 527499, Guangdong, China*)

Abstract: The catalytic activity of the catalysts is strongly dependent on the structure of the catalysts, and the exploration of their correlation and structure-controlled synthesis of the high-performance catalysts are always at the central. Currently, platinum (Pt) is the optimum catalyst for hydrogen evolution reaction (HER), oxygen reduction reaction (ORR) and alcohol oxidation reaction, while ruthenium (Ru) behaves as the champion catalyst for oxygen evolution reaction (OER) during water splitting. Preparing alloy catalysts with these precious metals can modulate the catalytic activity of these catalysts from the perspective of strain effect, ensemble effect and ligand effect. Here, we developed a strategy to deposit AuPt alloy as a solid solution phase on amorphous Ru supported on CNTs, thus forming AuPt-Ru heterostructures. The well-defined AuPt-Ru heterostructured catalysts were examined by X-ray diffraction and elemental mapping in high-angle annular dark-field scanning transition electron spectroscopy (HAADF-STEM). As compared to the high crystallinity AuPt alloy, AuPt alloy in AuPt-Ru heterostructure became amorphous, and AuPt-Ru showed superior catalytic activity toward ethanol oxidation reaction (EOR), achieving the mass activity of Pt as high as 21.44 $A \cdot mg^{-1}$ due to the high tolerance toward the poisoning species. The intermediates species of the EOR were also examined by *in-situ* FTIR spectroscopy. The stability of the catalysts toward EOR was also excellent and the degradation in the activity of the catalysts was strongly related to the loss of Ru content during the stability test. The heterostructured AuPt-Ru catalysts also exhibited the excellent alkaline HER and OER performances, superior to those of commercial Pt/C and RuO_2 catalysts, ascribing to the amorphous state of AuPt-Ru heterostructure, and the modulation by strain and ensemble effects. This work highlights the importance in the design of the multicomponent heterostructures for the synthesis of high-performance and multifunctional electrocatalysts.

Key words: ruthenium; AuPt Alloy; heterostructure; ethanol oxidation; hydrogen evolution; oxygen evolution; fuel cell

1 Introduction

Fuel cells represent the most prominent energy sources for electric vehicles and portable electric devices have been attracting extensive attention from the research communities[1]. However, there are still plenty of challenges to be overcome for the high-performance and cost-effective fuel cells devices for their eventual commercial application[2]. Among these, rational design and controlled synthesis of the high-performance electrocatalysts towards fuel cell relevant reactions are at the heart[3,4].

Currently, platinum (Pt) is the most commonly used electrocatalyst for the oxygen reduction reaction (ORR)[5], hydrogen oxidation and methanol/ethanol oxidation[6] of fuel cell relevant reactions, and also for hydrogen evolution reaction (HER)[7] in electrocatalyt-

Cite as: Gan T J, Wu J P, Liu S, Ou W J, Ling B, Kang X W. Low-crystalline and heterostructured AuPt-Ru@CNT as highly efficient multifunctional electrocatalyst. *J. Electrochem*., 2022, 28(8): 2201241.

Received: 2022-01-25, Revised: 2022-02-18. *Corresponding author, Tel: (86-20)39380520, E-mail: esxkang@scut.edu.cn

ic water splitting, while ruthenium (Ru) and iridium (Ir) based catalysts are recognized as the best catalysts for oxygen evolution reaction (OER)[4] during electrocatalytic water splitting[8]. Tremendous efforts have been devoted to the synthesis of Pt-based electrocatalysts. For example, shape-controlled synthesis can expose specific surface facets of metal nanocrystals, where the surface atoms with varied coordination numbers and environment can effectively modulate the catalytic activity of the catalysts[9]. In addition, surface and interface engineering are another powerful strategies in improving the catalytic activity of the catalyst due to the ensemble effect[10], surface strain effect[11], etc.

Alloying with other metals is also considered as an efficient strategy in decreasing the cost of precious metal-based electrocatalyst and simultaneously improving electrocatalytic activity[12]. The introduction of highly oxophilic metals (such as Ni, Co and Cu) can decrease the CO poisoning of the electrocatalyst due to the bifunctional mechanism[9,13], and the incorporation of Au into Pt catalysts can lead to profound enhancement of both electrocatalytic activity and stability of electro-oxidation of ethanol[14].

Most importantly, the synthesis of multicomponent alloy electrocatalysts may achieve multifunctional activity toward ORR, HER, OER, etc.[15] by synthesizing Pt, Au, Pd, Co, Ni and Ru, etc. based electrocatalyst simultaneously achieve high-performance electrocatalyst toward all these fuel cell relevant reactions. As to the alloy catalyst, it could be in form of the solid solution, core-shell and hetero-structure, where the ensemble effect, ligand effect and strain effect could play different roles in modulating the catalytic activity of the catalysts[16].

The catalytic activity of the metal catalyst can be also modulated by the crystallinity. It is reported that amorphous materials generally show enhanced catalytic performance in relative to crystalline catalysts due to their unique structures, such as abundant defects and unsaturated coordination sites on the surface. For example, Zhang et al. successfully prepared amorphization of layered crystalline $Pd_3P_2S_8$ that exhibited excellent electrocatalytic activity for HER[17]. Sargent et al. reported amorphous gelled FeCoW oxyhydroxides displaying a remarkable performance for OER in an alkaline electrolyte compared with those crystalline counterparts[18].

Au, Pt and Ru composite alloys have been widely reported due to their excellent electrochemical performance. The mixed solid solution[19] and core-shell structure have been deeply investigated. Atomic thin Pt-Ru shells were deposited on Au nanowires and used as electrocatalysts for methanol oxidation, where the Au can induce extensive strain towards the PtRu shells. The combination of Pt-Ru can effectively suppress the CO poisoning during methanol oxidation and thus promote reaction activity[20]. Ru@RuPt also remarkably outperforms Pt/C for alkaline HER[21]. However, the synthesis of heterostructured multiple-component electrocatalyst and the exploration of the regulation mechanism are very limited.

Herein, low crystalline and heterostructured AuPt-Ru alloys supported on CNTs, denoted as $(AuPt)_{0.5}$-Ru/CNTs, were prepared by sequential ethanol reduction method, and were further subject to the characterizations by XRD and high angle annular dark field (HAADF)-transmission electron microscopy (TEM). The catalytic activity of heterostructured $(AuPt)_{0.5}$-Ru/CNTs toward electrochemical EOR, alkaline HER and OER were examined in details, and the effects on the catalytic performance of the element component are discussed.

2 Experimental Section

2.1 Materials

Chloroplatinic acid ($H_2PtCl_6 \cdot 6H_2O$, 99%), gold acid chloride trihydrate ($HAuCl_4 \cdot 3H_2O$, 99%), ruthenium trichloride ($RuCl_3$, 99%), potassium hydroxide (KOH, 95%), absolute ethanol (CH_3CH_2OH, 99%), and sodium hydroxide (NaOH, 97%) were purchased from Energy Chemical Co. The support material, multiwall carbon nanotubes (CNTs, diameter: 10 ~ 20 nm), was purchased from Shenzhen Nanotech Port Co. Deionized (DI) water (18.2 MΩ·cm) was used in all experiments.

2.2 Preparation of Heterostructured $(AuPt)_{0.5}$-Ru on CNTs

A sequential ethanol reduction method was applied

to prepare CNTs-supported heterostructured AuPt-Ru nanoparticles. First, Ru nanoparticles were prepared on CNTs. Briefly, 200 mg CNTs and 83 mg $RuCl_3$ were dispersed into 130 mL absolute ethanol, heated to 110 ºC in an oil bath at a stirring rate of 300 r·min^{-1} and refluxed for 1 h. Then, 6 mL 0.2 mol·L^{-1} NaOH solution was added into the above solution and stirred for another 2 h for reduction. Finally, to ensure the complete reduction of Ru^{3+} ions, an extra 2 mL 0.2 mol·L^{-1} NaOH solution was further added into the above solution and stirred for another 30 min. The products were precipitated by centrifugation, washed three times with DI water and ethanol, respectively, and finally dried in a vacuum oven at 60 ºC. The obtained product is denoted as Ru/CNTs.

The heterostructured $(AuPt)_{05}$-Ru/CNTs sample was obtained by concurrent reduction of AuPt alloy at the atomic ratio of Au:Pt = 1:1 on Ru/CNTs using the ethanol reduction method. Firstly, 60 mg of Ru/CNTs was dispersed in absolute ethanol (25 mL) solution, heated to 80 ºC and stirred at a rate of 300 r·min^{-1}. Subsequently, 4 mL 0.2 mol·L^{-1} NaOH solution was added into the above solution and stirred for 30 min. Then, $H_2PtCl_6 \cdot 6H_2O$ and $HAuCl_4 \cdot 3H_2O$ at an atomic ratio of 1:1 in 20 mL ethanol solution were added into the above solution at a rate of 5 mL·h^{-1} and maintained at 80 ºC for 1.5 h. After cooling down to room temperature, the catalysts were collected by centrifugation, washed three times with DI water and absolute ethanol, respectively, and dried in a vacuum oven at 60 ºC for 24 h. The obtained samples are denoted as $(AuPt)_{0.5}$-Ru/CNTs. The RuAuPt mixed alloy NPs at the atomic ratio of Ru:Au:Pt = 1:0.25:0.25 were prepared by the similar process, where the mixed precursor solution of $RuCl_3$, $H_2PtCl_6 \cdot 6H_2O$ and $HAuCl_4 \cdot 3H_2O$ in ethanol was reduced concurrently at 80 ºC. As the control sample, AuPt/CNTs sample was equally prepared by following the same procedure without using $RuCl_3$ precursors.

2.3 Characterizations

Powder X-ray diffraction (XRD, Bruker D8 Advanced, German) measurement was carried out with a Cu K_α radiation source. X-ray photoelectron spectroscopy (XPS, PHI X-tool, Japan) using Al K_α as X-ray source was applied to detect the chemical state of samples. The morphology and the element distribution of the products were performed in high-angle annular dark-field scanning transition electron spectroscopy (HAADF-STEM).

2.4 Electrochemical Measurements

The catalysts were dispersed and sonicated in ethanol for 1 h to make a 1 mg·L^{-1} homogeneous catalyst ink. Then, 15 μL of catalyst ink was dropped on the glassy carbon electrode (6 mm in diameter). After evaporating the solvent naturally in air, 10 μL of 2wt% Nafion solution was drop cast on top of the catalyst and dried naturally in air. The electrochemical performance was investigated on a CHI-660E electrochemical workstation by using a standard three-electrode cell. The catalyst-covered glassy carbon electrode served as the working electrode and the platinum-wire electrode was used as the counter electrode. The electrocatalytic performance toward ethanol oxidation was carried out in 1.0 mol·L^{-1} ethanol and 1.0 mol·L^{-1} KOH aqueous solution in a potential window from -0.85 to 0.2 V (vs. Hg/HgO) through cyclic voltammetry at a scanning rate of 50 mV·s^{-1} and mercury/mercurous oxide electrode (Hg/HgO) was employed as the reference electrode. The electrocatalytic activity toward alkaline hydrogen evolution and oxygen evolution was performed in 1.0 mol·L^{-1} KOH aqueous solution by linear sweep voltammetry at a scan rate of 10 mV·s^{-1}. The stability of the electrocatalyst was evaluated by chronoamperometry (CA) for 1200 s at 0.7 V (vs. RHE). The electrochemical surface area (ECSA) of the catalysts was determined by CO stripping, which was acquired in 0.1 mol·L^{-1} $HClO_4$ aqueous solution by following the procedures below. The 0.1 mol·L^{-1} $HClO_4$ aqueous solution was first degassed with N_2 for 30 min. Then CA data were acquired at 0.1 V (vs. RHE) with the solution purged with CO for 5 min and then N_2 for another 20 min. The two CV scans were measured with a scan rate of 5 mV·s^{-1}. The mass activity for all the catalysts toward ethanol oxidation was evaluated by normalizing the current to the Pt loading. IR compensation was

performed for all the electrochemical measurements.

3 Results and Discussion

The XRD patterns of the as-prepared Ru/CNTs, AuPt/CNTs, $(AuPt)_{0.5}$-Ru/CNTs and RuPtAu/CNTs are shown in Figure 1. The Ru/CNTs displayed a broad peak of Ru(101) at 43.7° due to the presence of amorphous Ru nanoparticles (NPs), which was well observed for $(AuPt)_{0.5}$-Ru/CNTs [22], while the $(AuPt)_{0.5}$-Ru/CNTs displayed a peak at 38.89° corresponding to AuPt (111). The peak associated to AuPt (111) and observed from the $(AuPt)_{0.5}$-Ru/CNTs was located between Au (111) and Pt (111), and closer to that of Pt (111), indicating the formation of Au-Pt alloy. The smaller Bragg angle shift of the AuPt(111) peak for the $(AuPt)_{0.5}$-Ru/CNTs to that of Pt (111) indicates that the formation of Au-Pt alloy on the amorphous Ru NPs induces expansive strain on Pt. The interplanar spacing of the AuPt (111) reflection for the $(AuPt)_{0.5}$-Ru alloy NPs was calculated to be 2.314 Å [22]. Interestingly, the AuPt/CNTs displayed a sharper AuPt (111) peak than the $(AuPt)_{0.5}$-Ru. This suggests that the deposition of AuPt on the amorphous Ru NPs resulted in more amorphous AuPt nanocrystallites than AuPt NPs. The AuPt (111) peak in the pristine AuPt/CNTs was closer to Au (111), indicating a more expansive strain imposed on Pt.

Figure 2(a-b) shows the typical transmission electron microscopic (TEM) images of the $(AuPt)_{0.5}$-Ru/CNTs, which display spherical shapes with a diameter of 5.3 ± 0.2 nm and are evenly loaded on CNTs. The distance of the adjacent fringes was measured to be 2.32 Å in the HRTEM image (Figure 2(b)), consistent with the XRD result. This interplanar distance of AuPt (111) for the $(AuPt)_{0.5}$-Ru is larger than that of Pt(111) (2.27Å), further confirming the expansive strain induced on Pt by the heterostructured $(AuPt)_{0.5}$-Ru NPs. Moreover, a faded diffuse ring in the selected area electron diffraction (SAED) pattern (the inset in Figure 2(b)) was attributed to the amorphous character of Ru NPs. The energy dispersive X-ray (EDX) elemental mapping images (Figure 2(c-e)) revealed that Au and Pt elements overlapped with each other very well, indicating that the two elements are homogeneously mixed and form AuPt solid solution alloy. However, Ru, Au and Pt were observed on the same NPs, but did not overlap very well with each other (Figure 2(f)). This indicates that heterostructured (AuPt)-Ru, instead of Ru@AuPt core-shell structure or evenly mixed RuAuPt alloy were formed.

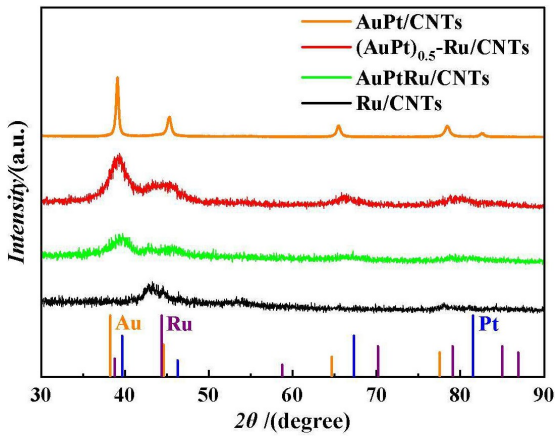

Figure 1 XRD profiles of Ru/CNTs, AuPt/CNTs, $(AuPt)_{0.5}$-Ru/CNTs and RuPtAu/CNTs. (color on line)

EOR activities of all the catalysts were evaluated in 1 mol·L^{-1} KOH containing 1 mol·L^{-1} ethanol, using cyclic voltammetry (CV), sweeping from 0.072 V to 1.12 V (vs. RHE) at a scan rate of 50 mV·s^{-1}. As shown in Figure 3(a), all these catalysts displayed the similar forward peak potential around 0.85 V. As shown in Figure 3(b), the peak current density of $(AuPt)_{0.5}$-Ru/CNTs was 21.4 A·mg^{-1}_{Pt}, which is much higher than those of AuPt/CNTs (2.69 A·mg^{-1}_{Pt}), RuPtAu/CNTs (0.92 A·mg^{-1}_{Pt}) and Pt/C (0.51 A·mg^{-1}_{Pt}), indicating the excellent electrocatalytic activity toward EOR. In the backward scan, the highest peak current density was also observed on the $(AuPt)_{0.5}$-Ru/CNTs (4.44 A·mg^{-1}_{Pt}), which is 16.7 times to that of the RuPtAu/CNTs. As shown in Figure 3 (a), the onset potential of the $(AuPt)_{0.5}$-Ru/CNTs was much lower than that of the RuPtAu/CNTs, indicating the enhanced kinetics of EOR for the $(AuPt)_{0.5}$-Ru/CNTs. Moreover, the $(AuPt)_{0.5}$-Ru/CNTs exhibited a much higher J_f/J_b (J_f and J_b represent the forward and backward peak current densities, respectively) ratio as compared with that of the RuPtAu/CNTs alloy catalysts (Table 1). This indicates that Ru-doping can sufficiently suppress the

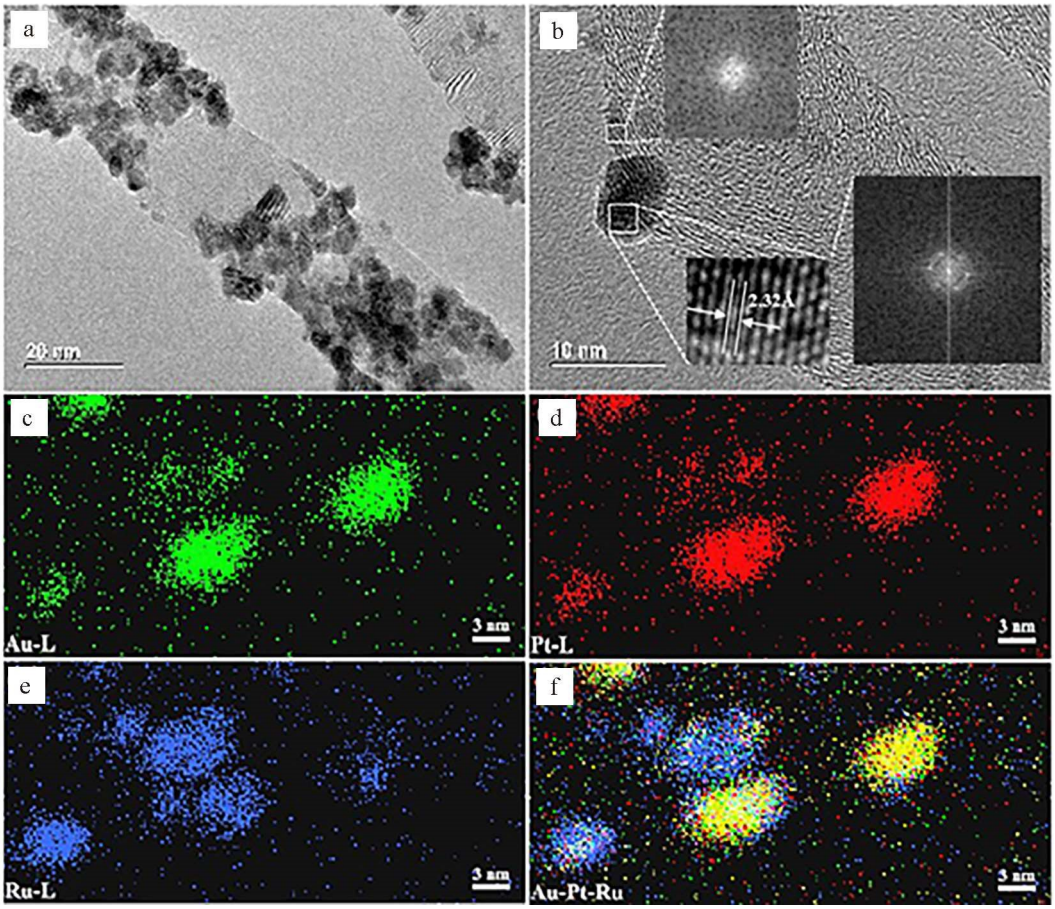

Figure 2 (a-b) TEM and (c-e) EDX-mapping images of Au, Pt, Ru, and (f) overlap of Au, Pt and Ru of $(AuPt)_{0.5}$-Ru/CNTs. (color on line)

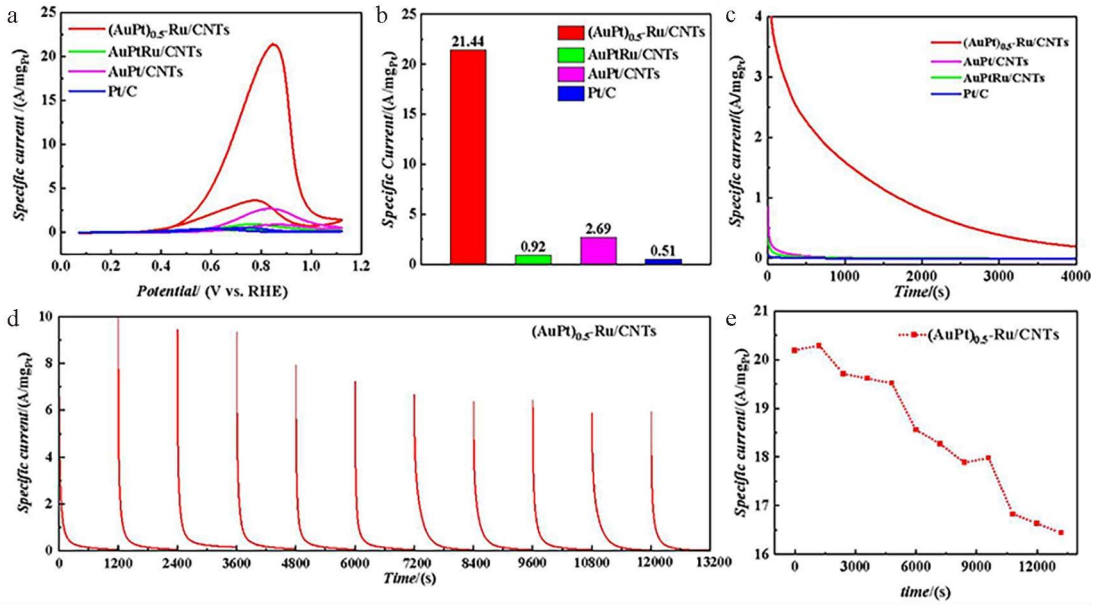

Figure 3 (a) EOR CV curves and (b) EOR peak currents in 1 mol·L^{-1} KOH with 1 mol·L^{-1} ethanol at a scan rate of 50 mV·s^{-1}. (c) chronoamperometric *i-t* curves of Pt/CNTs, AuPt/CNTs, $(AuPt)_{0.5}$-Ru/CNTs and RuPtAu/CNTs catalysts. (d) repeated chronoamperometric *i-t* curves at 0.7 V versus RHE and (e) CV curves after each *i-t* measurement of $(AuPt)_{0.5}$-Ru/CNTs. (color on line)

Table 1 Comparison in the activity of ethanol oxidation for the AuPt/CNTs, $(AuPt)_{0.5}$-Ru/CNTs and RuPtAu/CNTs catalysts, as well as Pt/C catalyst.

Catalyst	J_{peak}, A·mg_{Pt}^{-1}	J_f/J_b ratio
RuAuPt/CNTs	0.92	3.47
AuPt/CNTs	2.69	3.02
$(Au_5Pt_5)_{0.5}$-Ru/CNTs	21.4	4.82
Pt/C	0.51	1.25

poisoning effect for EOR and the heterostructured AuPt-Ru amorphous NPs are more efficient in the $(AuPt)_{0.5}$-Ru/CNTs[23].

In order to investigate the stability of the prepared catalysts toward electro-oxidation of ethanol, chronoamperometric (CA) tests were carried out at 0.7 V (vs. RHE) for 4000 s. As shown in Figure 3(c), there was a sharp decline in the current density during the first 500 s, which has been ascribed to the adsorption of poisoning intermediates formed at the beginning of the EOR. In comparison with Pt/C, AuPt/CNTs and RuPtAu/CNTs, the $(AuPt)_{0.5}$-Ru/CNTs displayed the highest stability and prolonged duration. The high activity of $(AuPt)_{0.5}$-Ru toward EOR might be strongly related to the amorphous-like state of AuPt in the heterostructured $(AuPt)_{0.5}$-Ru.

We have further studied the catalytic activity and durability of the $(AuPt)_{05}$-Ru/CNTs by CA experiments at 0.7 V (vs. RHE), and the results are presented in Figure 3(d). After each chronoamperometric test for 1200 s, the $(AuPt)_{0.5}$-Ru/CNTs catalyst was reactivated by five consecutive CV cycles in 1 mol·L^{-1} KOH solution, and followed by another CA test in a fresh 1 mol·L^{-1} KOH electrolyte containing 1 mol·L^{-1} ethanol. More impressively, after reactivation, the $(AuPt)_{05}$-Ru/CNTs could recover its original EOR activity. After 11 consecutive cycles (13200 s), the drop of the EOR activity was less than 20%, indicating the outstanding durability. Figure 4 displays the elemental mapping at the atomic scale of the $(AuPt)_{0.5}$-Ru/CNTs after the repeated chronoamperometric and CV tests for EOR, only minor amount of Ru was observed as compared to those of Au and Pt. This could indicate that the loss of the EOR activity of this catalyst might come from the loss of Ru during the test.

To gain deep insight into the high catalytic activity of the $(AuPt)_{0.5}$-Ru/CNTs catalyst, *in-situ* FTIR spectroscopy was applied to identify the intermediates and products of ethanol oxidation. Figure 5 shows the

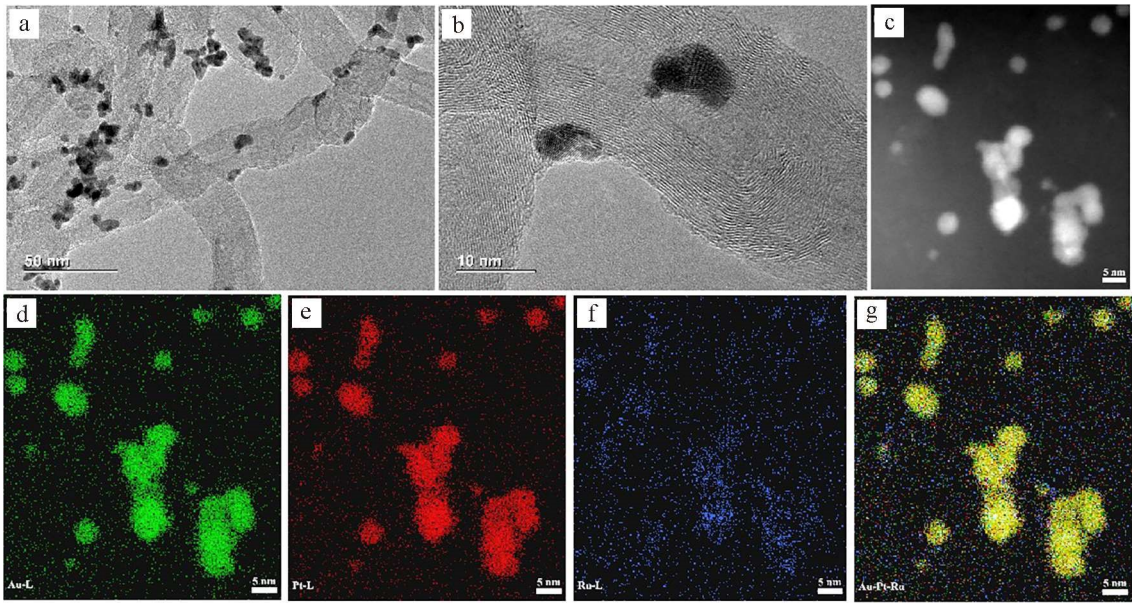

Figure 4 (a-b) TEM images and (c-f) EDX-mapping images of Au, Pt, Ru and (g) overlap profile of Au, Pt and Ru elements of $(AuPt)_{0.5}$-Ru/CNTs after EOR test. (color on line)

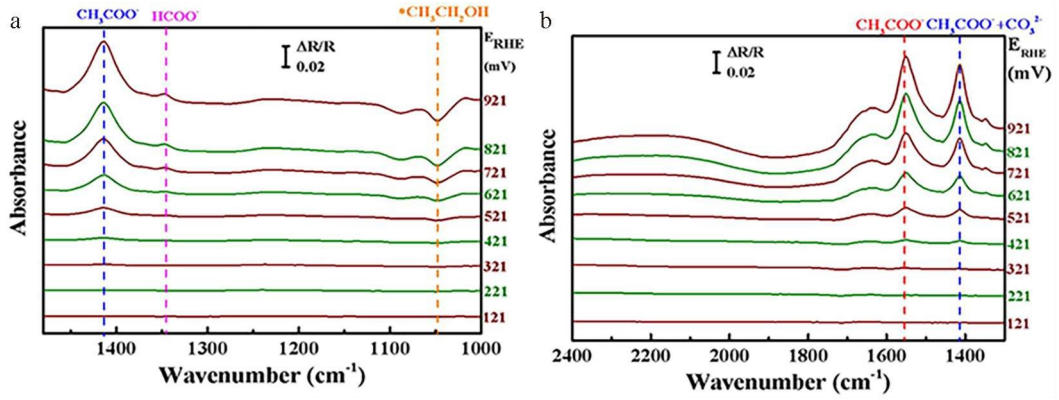

Figure 5 *In-situ* FTIR spectra of EOR on the $(AuPt)_{0.5}$-Ru/CNTs catalyst at the 1st run in 1 mol·L^{-1} KOH containing 1 mol·L^{-1} EtOH

in-situ FTIR spectra of ethanol oxidation in 1.0 mol·L^{-1} ethanol and 1.0 mol·L^{-1} KOH solution recorded at different potentials. Two major IR bands at 1550 cm^{-1} and 1415 cm^{-1} were attributed to the asymmetric and symmetric C-O bonds stretching vibrations, respectively, which are characteristic of acetate ions (CH_3COO^-)[24]. Note that at high pH environment, the main soluble product (CO_2) from the complete ethanol oxidation existed in the form of carbonate (CO_3^{2-}), which displays a band at 1390 cm^{-1} and overlaps with the band of 1418 cm^{-1} from acetate[25]. The COO^- stretching vibrations corresponding to formate species ($HCOO^-$) were observed at 1340 cm^{-1}[26]. The IR band at 1044 cm^{-1} belonged to C_2H_5OH, which can be applied to monitor the adsorbed ethanol.

Furthermore, the electrocatalytic performances of $(AuPt)_{0.5}$-Ru/CNTs toward alkaline HER and OER were evaluated by LSV in 1 mol·L^{-1} KOH solution, and compared with those of the AuPtRu/CNTs, AuPt/CNTs and Pt/C, as shown in Figure 6(a-c). It is clearly observed that the $(AuPt)_{0.5}$-Ru/CNTs exhibited the best HER performance among these samples. The

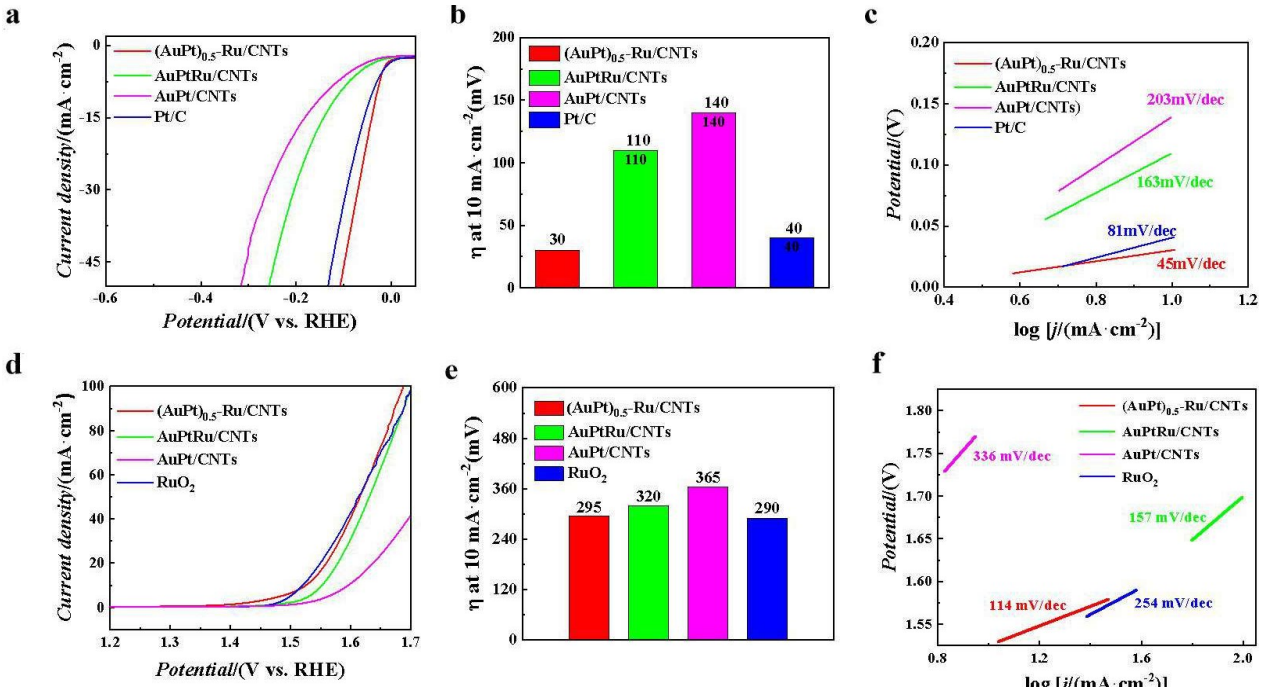

Figure 6 HER (a-c) and OER (d-f) performances. (a, d) LSV curves, (b, e) overpotential (η_{10}) plots @10 mA·cm^{-2}, and (c, f) Tafel plots for $(AuPt)_{0.5}$-Ru/CNTs, AuPtRu/CNTs, AuPt/CNTs, and Pt/C. (color on line)

$(AuPt)_{0.5}$-Ru/CNTs only required an overpotential (η_{10}) of 30 mV, which is 80, 110 and 10 mV lower than those of the AuPtRu/CNTs, AuPt/CNTs, and Pt/C, respectively. The $(AuPt)_{0.5}$-Ru/CNTs catalyst exhibited the fastest alkaline HER kinetics, as demonstrated by the smallest Tafel slope in Figure 6(c), namely, 45 mV·dec^{-1} for the $(AuPt)_{0.5}$-Ru/CNTs, 163 mV·dec^{-1} for the AuPtRu/CNTs, 203 mV·dec^{-1} for the AuPt/CNTs and 81 mV·dec^{-1} for Pt/C. These Tafel slopes indicate that the rate determining step is Heyrovsky step for the $(AuPt)_{0.5}$-Ru/CNTs and Pt/C, while Volmer step for the AuPtRu/CNTs and AuPt/CNTs.

It is usually believed that water dissociation kinetics is slower on Pt than the transition metals with more deficient d-electrons[27], such as Ru, Co and Ni. Thus, the introduction of Ru into AuPt alloy could promote water dissociation on the Ru site, while hydrogen desorption through the Heyrovsky step could occur on the Pt site[28]. It was found that the RuAuPt/CNTs exhibited better alkaline HER performance than the AuPt/CNTs. This suggests that the water dissociation dynamics are sufficiently improved upon the formation of the AuPt-Ru heterostructure. Usually, the doping of Ru into AuPt lattice could induce compressive strain and downshift of the d-band of Pt. While the formation of heterostructured AuPt with amorphous Ru can well maintain the original d-band of AuPt and its strong adsorption of water molecules. Most importantly, the amorphous Ru may behave as excellent water dissociation sites and the formation of the AuPt-Ru heterostructure may simultaneously promote alkaline HER.

The electrocatalytic performance of the $(AuPt)_{0.5}$-Ru/CNTs toward alkaline OER was examined and is compared with those of the AuPtRu/CNTs, AuPt/CNTs, and RuO_2 in 1 mol·L^{-1} KOH. As shown in Figure 6(d-f), the $(AuPt)_{0.5}$-Ru/CNTs exhibited higher OER performance than the AuPtRu/CNTs and AuPt/CNTs. The required η_{10} values were 295 mV, 320 mV, 365 mV, and 290 mV for the $(AuPt)_{0.5}$-Ru/CNTs, AuPtRu/CNTs, AuPt/CNTs, and Pt/C, respectively, as shown in Figure 6(e). It cannot be ignored that the $(AuPt)_{0.5}$-Ru/CNTs had better OER performance than the RuO_2 at the low current density (< 5 mA·cm^{-2}) and high current density (> 60 mA·cm^{-2}). Tafel slope of the $(AuPt)_{0.5}$-Ru/CNTs (114 mV·dec^{-1}) was also much lower than those of the other catalysts (Figure 6(f)), suggesting a very rapid OER reaction rate.

4 Conclusions

In summary, this work has demonstrated the successful synthesis of less crystallized and heterostructured $(AuPt)_{0.5}$-Ru nanomaterials supported on CNTs by sequential ethanol reduction method. The reduced crystalline state of AuPt alloy and formation of heterostructure were confirmed by XRD data and elemental mapping in HAADF-TEM. The $(AuPt)_{0.5}$-Ru/CNTs showed superior EOR performance, and the mass activity of Pt toward EOR was as high as 21.4 A·mg^{-1}, extremely higher than those of the previously reported catalysts in the literature, as well as those of the uniformly mixed AuPt and RuAuPt nanoparticles. The *in-situ* FTIR spectroscopic study identified the two IR bands at 1550 cm^{-1} and 1415 cm^{-1}, ascribing to the asymmetric and symmetric C-O bonds of acetate ions (CH_3COO^-), respectively, and the IR band at 1390 cm^{-1} from carbonate (CO_3^{2-}). The $(AuPt)_{0.5}$-Ru/CNTs also exhibited the excellent electrochemical stability and long-term durability in ethanol oxidation. The deactivation of the catalysts was accompanied by the loss of Ru contents, implying that Ru plays a crucial role in EOR activity. Concurrently, the $(AuPt)_{0.5}$-Ru/CNTs also displayed the excellent HER and OER activities in alkaline media, which was ascribed to the ensemble and strain effects of the amorphous and heterostructured metal alloy.

Notes:

The authors declare no competing financial interest.

Acknowledgements:

This work was supported by the National Natural Science Foundation of China (No. U2032151) and CSG Technology Project (No. GDKJXM20198054).

References:

[1] Deng R Y, Xia Z X, Sun R L, Wang S L, Sun G Q. Nanostructured ultrathin catalyst layer with ordered platinum nanotube arrays for polymer electrolyte membrane fuel cells[J]. J. Energy Chem., 2020, 43: 33-39.

[2] Han S H, Liu H M, Chen P, Jiang J X, Chen Y. Porous trimetallic PtRhCu cubic nanoboxes for ethanol electrooxidation[J]. Adv. Energy Mater., 2018, 8(24): 1801326.

[3] Zhuang Z H, Chen W. Application of atomically precise metal nanoclusters in electrocatalysis[J]. J. Electrochem., 2021, 27(2): 125-143.

[4] Tang T, Jiang W J, Niu S, Hu J S. Design strategies toward highly active electrocatalysts for oxygen evolution reaction[J]. J. Electrochem., 2018, 24(5): 409-426.

[5] Wang K L, Wang F, Zhao Y F, Zhang W Q. Surface-tailored PtPdCu ultrathin nanowires as advanced electrocatalysts for ethanol oxidation and oxygen reduction reaction in direct ethanol fuel cell[J]. J. Energy Chem., 2021, 52: 251-261.

[6] Yu Z Y, Huang R, Liu J, Li G, Song Q T, Sun S G. Preparation of PdCoIr tetrahedron nanocatalysts and its performance toward ethanol oxidation reaction[J]. J. Electrochem., 2021, 27(1): 63-75.

[7] Li Y, Luo Z Y, Ge J J, Liu C P, Xing W. Research progress in hydrogen evolution low noble/non-precious metal catalysts of water electrolysis[J]. J. Electrochem., 2018, 24(6): 572-588.

[8] Papaefthimiou V, Diebold M, Ulhaq-Bouillet C, Doh W H, Blume R, Zafeiratos S, Savinova E R. Potential-induced segregation phenomena in bimetallic PtAu nanoparticles: An *in-situ* near-ambient-pressure photoelectron spectroscopy study[J]. ChemElectroChem, 2015, 2(10): 1519-1526.

[9] Sulaiman J E, Zhu S Q, Xing Z L, Chang Q W, Shao M H. Pt-Ni octahedra as electrocatalysts for the ethanol electro-oxidation reaction[J]. ACS Catalysis, 2017, 7(8): 5134-5141.

[10] Erini N, Beermann V, Gocyla M, Gliech M, Heggen M, Dunin-Borkowski R E, Strasser P. The effect of surface site ensembles on the activity and selectivity of ethanol electrooxidation by octahedral PtNiRh nanoparticles[J]. Angew. Chem. Int. Ed., 2017, 56(23): 6533-6538.

[11] Zou J S, Wu M, Ning S L, Huang L, Kang X W, Chen S W. Ru@Pt core-shell nanoparticles: impact of the atomic ordering of the Ru metal core on the electrocatalytic activity of the Pt Shell[J]. ACS Sustain. Chem. Eng., 2019, 7(9): 9007-9016.

[12] Kowal A, Li M, Shao M, Sasaki K, Vukmirovic M B, Zhang J, Marinkovic N S, Liu P, Frenkel A I, Adzic R R. Ternary Pt/Rh/SnO_2 electrocatalysts for oxidizing ethanol to CO_2[J]. Nat. Mater., 2009, 8(4): 325-330.

[13] Wei Y C, Liu C W, Wang K W. Improvement of oxygen reduction reaction and methanol tolerance characteristics for PdCo electrocatalysts by Au alloying and Co treatment[J]. Chem. Commun., 2011, 47(43): 11927-11929.

[14] Liang Z X, Song L, Deng S Q, Zhu Y M, Stavitski E, Adzic R R, Chen J Y, Wang J X. Direct 12-electron oxidation of ethanol on a ternary Au(core)-PtIr(shell) electrocatalyst[J]. J. Am. Chem. Soc., 2019, 141(24): 9629-9636.

[15] Glasscott M W, Pendergast A D, Goines S, Bishop A R, Hoang A T, Renault C, Dick J E. Electrosynthesis of high-entropy metallic glass nanoparticles for designer, multi-functional electrocatalysis[J]. Nat. Commun., 2019, 10: 2650.

[16] Guo Z W, Kang X W, Zheng X S, Huang J, Chen S W. PdCu alloy nanoparticles supported on CeO_2 nanorods: Enhanced electrocatalytic activity by synergy of compressive strain, PdO and oxygen vacancy[J]. J. Catal., 2019, 374: 101-109.

[17] Zhang X, Luo Z M, Yu P, Cai Y Q, Du Y H, Wu D X, Gao S, Tan C L, Li Z, Ren M Q, Osipowicz T, Chen S M, Jiang Z, Li J, Huang Y, Yang J, Chen Y, Ang C Y, Zhao Y L, Wang P, Song L, Wu X J, Liu Z, Borgna A, Zhang H. Lithiation-induced amorphization of $Pd_3P_2S_8$ for highly efficient hydrogen evolution[J]. Nat. Catal., 2018, 1(6): 460-468.

[18] Zhang B, Zheng X L, Voznyy O, Comin R, Bajdich M, Garcia-Melchor M, Han L L, Xu J X, Liu M, Zheng L R, de Arquer F P G, Dinh C T, Fan F J, Yuan M J, Yassitepe E, Chen N, Regier T, Liu P F, Li Y H, De Luna P, Janmohamed A, Xin H L L, Yang H G, Vojvodic A, Sargent E H. Homogeneously dispersed multimetal oxygen-evolving catalysts[J]. Science, 2016, 352: 333-337.

[19] Kang X W, Miao K H, Guo Z W, Zou J S, Shi Z Q, Lin Z, Huang J, Chen S W. Pdru alloy nanoparticles of solid solution in atomic scale: Size effects on electronic structure and catalytic activity towards electrooxidation of formic acid and methanol[J]. J. Catal., 2018, 364: 183-191.

[20] Zhu X R, Hu Z, Huang M, Zhao Y X, Qu J Q, Hu S. Au nanowires with high aspect ratio and atomic shell of Pt-Ru alloy for enhanced methanol oxidation reaction[J]. Chinese Chem Lett, 2021, 32(6): 2033-2037.

[21] Wang X L, Cong Y Y, Qiu C X, Wang S J, Qin J Q, Song Y J. Core-shell structured Ru@PtRu nanoflower electrocatalysts toward alkaline hydrogen evolution reaction[J]. J. Electrochem., 2020, 26(6): 815-824.

[22] Hu X, Zou J S, Gao H C, Kang X W. Trimetallic Ru@AuPt core-shell nanostructures: The effect of microstrain on Co adsorption and electrocatalytic activity of formic acid oxidation[J]. J. Colloid Interf. Sci., 2020, 570: 72-79.

[23] Liu K, Wang W, Guo P H, Ye J Y, Wang Y Y, Li P T, Lyu Z X, Geng Y S, Liu M C, Xie S F. Replicating the defect structures on ultrathin Rh nanowires with Pt to

achieve superior electrocatalytic activity toward ethanol oxidation[J]. Adv. Funct. Mater., 2019, 29(2): 1806300.

[24] Yang G X, Farsi L, Mei Y H, Xu X, Li A Y, Deskins N A, Teng X W. Conversion of ethanol via C-C splitting on noble metal surfaces in room-temperature liquid-phase [J]. J. Am. Chem. Soc., 2019, 141(24): 9444-9447.

[25] Li H Q, Fan Q Y, Ye J Y, Cao Z M, Ma Z F, Jiang Y Q, Zhang J W, Cheng J, Xie Z X, Zheng L S. Excavated Rh nanobranches boost ethanol electro-oxidation[J]. Mater. Today Energy, 2019, 11: 120-127.

[26] Tan T H, Scott J, Ng Y H, Taylor R A, Aguey-Zinsou K F, Amal R. C-C cleavage by Au/TiO_2 during ethanol oxidation: Understanding bandgap photoexcitation and plasmonically mediated charge transfer via quantitative *in situ* drifts[J]. ACS Catalysis, 2016, 6(12): 8021-8029.

[27] Xie Y F, Cai J Y, Wu Y S, Zang Y P, Zheng X S, Ye J, Cui P X, Niu S W, Liu Y, Zhu J F, Liu X J, Wang G M, Qian Y T. Boosting water dissociation kinetics on Pt-Ni nanowires by N-induced orbital tuning[J]. Adv. Mater., 2019, 31(16): 1807780.

[28] Luo M, Cai J Y, Zou J S, Jiang Z, Wang G M, Kang X W. Promoted alkaline hydrogen evolution by an N-doped Pt-Ru single atom alloy[J]. J. Mater. Chem. A, 2021, 9(26): 14941-14947.

低结晶度 AuPt-Ru/CNTs 合金异质结作为高效多功能电催化剂

甘团杰[1],武建平[1],刘 石[2],区文俊[2],凌 彬[2],康雄武[2*]

(1. 广东电网有限责任公司江门供电局, 广东 江门 529030; 2. 广东慧氢能源科技有限公司, 广东 广州 527499)

摘要: 催化剂的活性与其结构紧密相关, 研究催化剂的构效关系以及可控合成高效电催化剂, 并探究其催化机制, 一直是科学研究的核心。贵金属铂是优异的电解水析氢的催化剂, 同时也是直接醇燃料电池阳极氧化的良好催化剂, 而贵金属钌是优异的电解水析氧催化剂。这些与燃料电池及氢能相关的重要反应催化剂, 可通过合成 Pt、Au 及 Ru 的合金催化剂, 通过应力效应、电子效应及团簇效应, 可有效提高金属催化剂的活性, 并实现多功能电催化性能。本文报道了可控合成低结晶度的 AuPt-Ru 合金异质结,并通过元素扫描分析及 X 射线衍射分析确认其结构。该催化剂表现出了非常优异的电催化氧化乙醇活性, 其归一化到 Pt 的质量活性达到了为 21.4 $A\cdot mg^{-1}_{Pt}$, 远远高于对照组样品 AuPt 及 RuAuPt 混合相催化剂及文献报道样品。催化剂同样表现出了非常好的乙醇氧化稳定性, 但是其活性的衰减与其 Ru 组分的流失紧密相关。我们同时通过电化学原位红外光谱,研究了该催化剂乙醇氧化中间产物, 分析了其反应机理。该催化剂同样表现出了优异的碱性电解水析氢及析氧催化活性, 其析氢电流 10 $mA\cdot cm^{-2}$ 对应的过电位为 30 mV, Tafel 斜率为 45 $mV\cdot dec^{-1}$, 优于 AuPt 及 RuPtAu 对照组样品。该催化剂优异的电化学性能主要归结于其低结晶度和异质结及其伴随的应力效应及团簇效应。本报道提供了一种可控合成具有异质结结构的金属合金催化剂, 突出了其对实现多功能、高性能合金电催化剂的重要性。

关键词: 钌; 异质结; AuPt 合金; 乙醇电氧化; 电解水析氢; 电解水析氧